www.czasopisma.pan.pl PAN POLSKA AKADEMIA NAUK www.journals.pan.pl

Arch. Metall. Mater. **65** (2020), 1, 157-162

DOI: 10.24425/amm.2019.131109

K. DOMAGAŁA[1,2*], M. BORLAF[1], D. KATA[2], T. GRAULE[1]

SYNTHESIS OF COPPER-BASED MULTI-WALLED CARBON NANOTUBE COMPOSITES

In this study, the synthesis of copper-based multi-walled carbon nanotube composites is described. Over the last years, carbon nanotubes (CNTs) have been widely used in many scientific research fields and have found applications in several sectors, e.g. for water treatment. This work focuses on combining the exceptional characteristics of CNTs, such as high specific surface area and antibacterial properties, with the antimicrobial/ antivirus features of copper oxides. The influence of synthesis parameters and thermal treatment on the final product was studied. Copper leakage was evaluated at both pH 5 and pH 7, confirming the possibility of applying Cu-based MWCNT composites in water filtration systems.

Keyword: MWCNT, water treatment, copper, cuprous oxide, cupric oxide

1. Introduction

Carbon nanotubes (CNTs) have gained a lot of interest over the last years and have become an important topic of scientific research due to their properties, such as remarkable mechanical and chemical strength, optical activity, thermal stability, thermal and electrical conductivity, as well as high surface area [1-3]. These characteristics have led to their wide application in many different fields of science and innovative technologies [3-5], e.g. optoelectronics, semiconductors, catalysts, biochemistry and water purification [2,3,6,7] due to their strong antimicrobial properties [8-11]. In a recent research, Brady-Estevez at al. [12] developed a multi-walled carbon nanotube (MWCNT) filter, which allowed for a great exclusion of Escherichia coli (E. coli) bacteria and MS2 bacteriophage viruses from water. According to the mentioned study [12,13], MWCNTs have shown significantly better virus removal properties compared to single-walled carbon nanotubes (SWCNT).

For water purification applications, MWCNTs are rarely used in pure form, however, they have been used in the form of composites, dispersed in polymers or functionalised with metallic nanoparticles [2]. With the incorporation of metal oxides, the surface charge changes, leading to electrostatic interactions that increase the sorption capacity of MWCNTs [2]. This is a crucial characteristic as the removal of viruses is based on electrostatically enhanced adsorption [6,14,15]. CNTs for water treatment applications can be functionalised with metal or metal oxides, most commonly Fe_2O_3/Fe_3O_4 [16], Al/Al_2O_3 [17], TiO_2 [18] and Ag [3,19]. Such modified composites have exhibited improved virus adsorption and disinfection properties [3,6].

Cupric oxide (CuO) and cuprous oxide (Cu_2O) have been reported to be suitable antimicrobial and antivirus agents [20-22]. The main advantages of copper oxides over other metallic oxides are their stable physical and chemical properties, as well as low manufacturing costs [20].

The aim of this work was to prepare Cu-based/MWCNT composites via chemical precipitation for virus removal applications, as well as to study the influence of synthesis parameters and thermal treatment on the final product. Additional investigations were performed to evaluate the possible application of the Cu-based/MWCNT composites as a water filter by studying the copper leakage.

2. Materials and methods

2.1. Materials

The MWCNTs were purchased from Cheap Tubes (USA). Copper (II) acetate monohydrate ($Cu[CH_3COO]_2 \times H_2O$ (Sigma-Aldrich) was used as the copper oxide precursor, tetramethylammonium hydroxide (TMAH, $N(CH_3)_4$ (OH), Sigma-Aldrich) as the precipitating agent and nanopure water as the reaction medium (18.2 MΩ, MicroPure UV, Thermo Scientific).

[1] LABORATORY FOR HIGH PERFORMANCE CERAMICS, EMPA, SWISS FEDERAL LABORATORIES FOR MATERIALS SCIENCE AND TECHNOLOGY, DÜBENDORF, SWITZERLAND
[2] AGH UNIVERSITY OF SCIENCE AND TECHNOLOGY, FACULTY OF MATERIALS SCIENCE AND CERAMICS, AL. MICKIEWICZA 30, 30-059 KRAKOW, POLAND

* Corresponding author: kamila.domagala@empa.ch

2.2. Synthesis of Cu-based/MWCNT composites

The first step was to modify the MWCNTs via chemical oxidation to oxidise the carbon present on the surface of the MWCNTs to carboxylic groups [2,23-26]. The surface functionalisation was carried out by dispersing the MWCNTs (applying 5 min of water bath ultrasonication, DT106, Bandelin Electronics) in concentrated nitric acid (HNO_3 70%, (Sigma-Aldrich) and leaving them under stirring for 24 h at room temperature. After that, the dispersion was filtered and washed using nanopure water until a neutral pH was obtained. The filtered MWCNTs were dried overnight in an oven (FD-115, Binderat) at 120°C.

The precursor solution was prepared by dissolving 2.82 g of copper acetate hydrate in 50 mL of nanopure water. Afterwards, the functionalised MWCNTs were added to the solution and sonicated for 5 min. Then, TMAH was added at a rate of 10 mL/min using a syringe pump (PHD ultra CP, Harvard Apparatus GmbH) under continuous stirring (300 rpm). After 24 h, the Cu-based/MWCNT composite was filtered by vacuum filtration and dried in an oven at 120°C for 2 h. Finally, the prepared material was calcinated in a tube furnace (GHC 120900, Carbolite Gero GmbH & Co. KG) at various temperatures (300, 400 and 500°C) for 2 h under N_2 atmosphere.

2.3. Characterisation

Unmodified MWCNTs and Cu-based/MWCNT materials were characterised using Raman spectroscopy with backscattering geometry, using an Alpha 300 R Confocal Raman Microscope (WITec) working at λ = 532 nm. X-ray diffraction (XRD) analyses were carried out to determine the crystal phases using PANalytical X'Pert PROh-2h (PANalytical) scan system equipped with a Johansson monochromator (Cu Kα1 radiation, 1.5406 Å) and a X'Celerator linear detector. The crystal sizes (S) were calculated using the Scherrer equation (Eq. 1):

$$S = \frac{k\lambda}{\beta \cos\Theta} \tag{1}$$

where: k – shape factor (0.9), λ – X-ray wavelength, β – full width at half-maximum intensity (radians), and θ – Bragg angle (degrees).

Transmission Electron Microscope (TEM, JEOL JEM-2200FS) working at an accelerating voltage of 200 kV, was used to investigate the size, morphology and distribution of the studied material. Samples were prepared by dispersing the material in ethanol and sonicating for 2 min. A few drops of the dispersion were deposited onto carbon-coated copper grids (S166-2 model, Plano). The specific surface area (SSA) was measured by means of BET isotherm, using a Beckman-Coulter SA3100 instrument. The release of copper during the filtration process was determined via the inductively coupled plasma-mass spectrometry (ICP-MS, Spectro Element 2, Thermo Fisher Scientific) technique. Copper leakage tests were carried out by rinsing 100 mg Cu-based composites deposited on a glass fibre filter (0.4 µm, Mancherey-Nagel, Switzerland) with nanopure water at pH values of 5 and 7 (adjusted with 0.01 M NaOH standardised solution, Sigma-Aldrich).

3. Results and discussion

3.1. MWCNT characterisation

In Figure 2 a series of TEM images recorded at different magnifications of the as-received MWCNTs show agglomerated nanotubes in the form of a bundled network. The outer and inner diameters are in the range of 10-25 nm and 3-5 nm, respectively

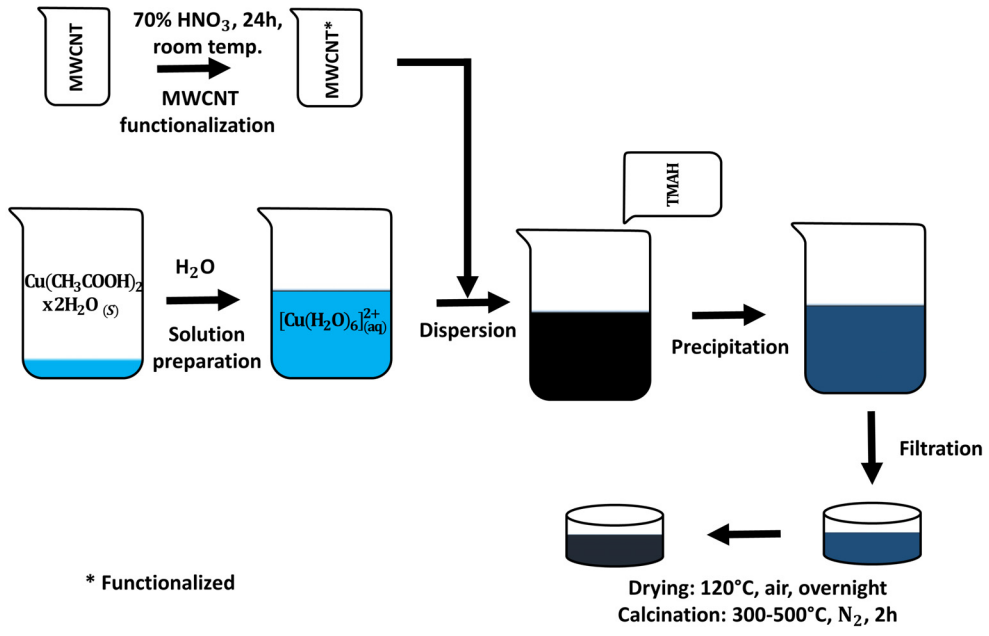

Fig. 1. Scheme of the Cu-based composite synthesis

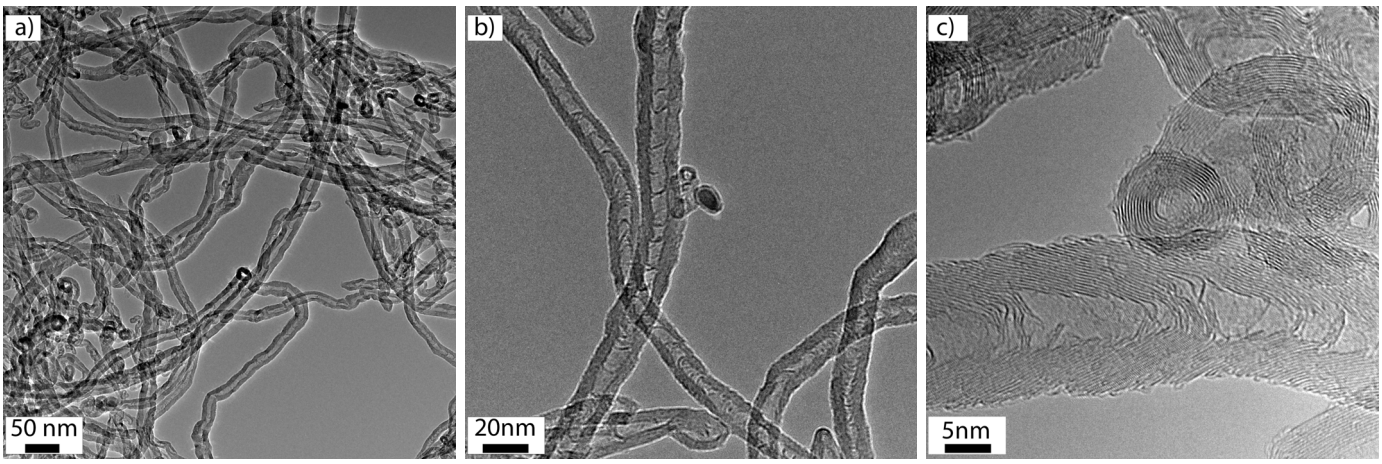

Fig. 2a, b and c. A series of TEM images of pristine MWCNTs recorded at different magnifications

(Figs. 2b and c). Moreover, the multi-walled structure of the CNT can be observed, with the wall thicknesses being in the range of 2-4 nm. Those results and the measured SSA = 117 m^2/g are in good agreement with the information provided by the supplier. The Raman spectrum, shown in Figure 3, revealed the characteristic bands of MWCNT. At 1345 cm^{-1} the D band associated with the defect in the carbon with sp^2 hybridisation was observed [27]. The peak is very prominent, confirming the high defective level of the material's structure [28]. At ~1600 cm^{-1} the G band is observed, which is composed of two bands centered at ~1580 cm^{-1} (G) and ~1612 cm^{-1} (D'). The G band is assigned to the graphitisation of the sample, circumferential displacement and in-plane vibration of the C-C bond in all sp^2 carbon materials [27]. Meanwhile, the D' band provides information about the atomic displacement along the nanotube axis [27]. The G*, G', D + G and 2D' bands are also observed at 2450 cm^{-1}, 2690 cm^{-1}, 2930 cm^{-1} and 3210 cm^{-1}, respectively, whose intensities increase with the number of defects [29]. Finally, the ratio between the area of the D and G bands is relatively high (D/G = 1.55), indicating that many defect points are present in the as-received MWCNTs, which may potentially lead to the CNT surface modification.

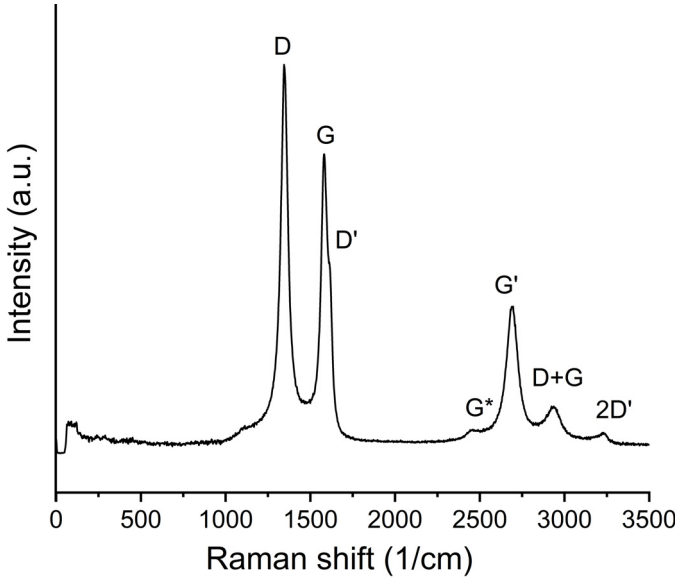

Fig. 3. Raman spectrum of pristine MWCNTs

3.2. Synthesis and characterisation of Cu-based/MWCNT composites

Once copper acetate is dissolved in water, an aqueous complex (Eq. 2) [30] forms, resulting in a solution with a characteristic light blue colour. Subsequently, the MWCNTs were dispersed and then, the TMAH was added in stoichiometric amount. This caused the aqueous complex to precipitate the copper hydroxide (Eq. 3) [[30]], characterised by a pale-blue colour.

$$Cu(CH_3COO)_{2(s)} \xrightarrow{H_2O} \left[Cu\left(H_2O\right)_6\right]^{2+}_{(aq)} + 2CH_3COO^-_{(aq)} \quad (2)$$

$$\left[Cu\left(H_2O\right)_6\right]^{2+}_{(aq)} + 2OH^-_{(aq)} \rightarrow Cu\left(OH\right)_{2(s)} + 6H_2O \quad (3)$$

$$Cu\left(OH\right)_{2(s)} \xrightarrow{\Delta} CuO_{(s)} + H_2O \quad (4)$$

Figure 4 presents the XRD pattern of the reaction product (Eq. 3) in the absence of MWCNTs before (after the drying process) and after calcination. As expected, after drying, only the $Cu(OH)_2$ phase was observed, however, after the thermal treatment at 300°C under N_2 atmosphere, both Cu_2O and CuO phases were detected, where the majority was Cu_2O (63%).

In the case of the synthesis performed in the presence of MWCNTs, the reaction product is quite different after calcination, with Cu_2O being the dominant phase (Fig. 5). However, when excess of TMAH was added, the amount of CuO increased, obtaining similar results to the synthesis without MWCNTs. Taking into account the lower solubility of Cu_2O compared to CuO below 150°C [31], the use of the stoichiometric amount was chosen to obtain Cu_2O/MWCNT composites.

Figure 6 shows the influence of calcination temperature on the synthesis product. In general, the amount of CuO decreases

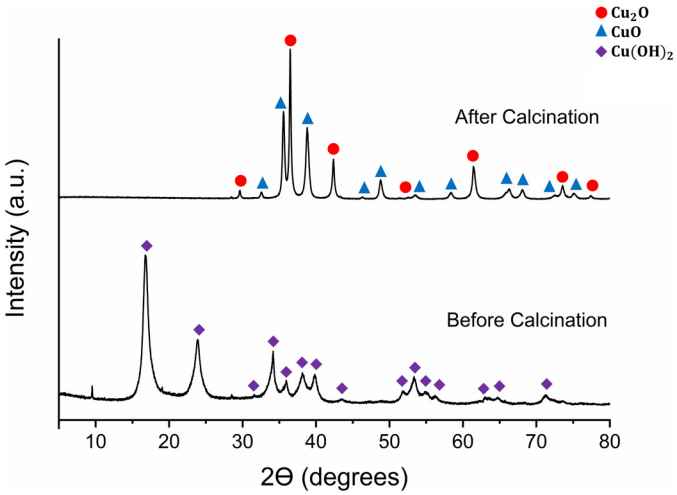

Fig. 4. XRD patterns of the reaction product before and after thermal treatment

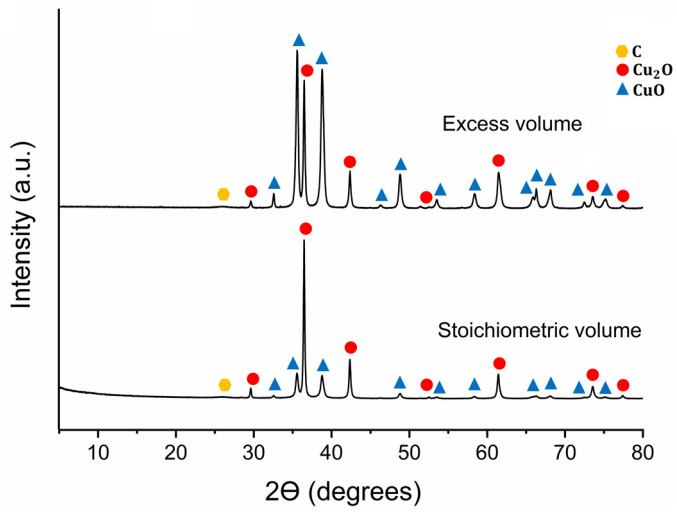

Fig. 5a. XRD patterns of the Cu-based/MWCNT composites

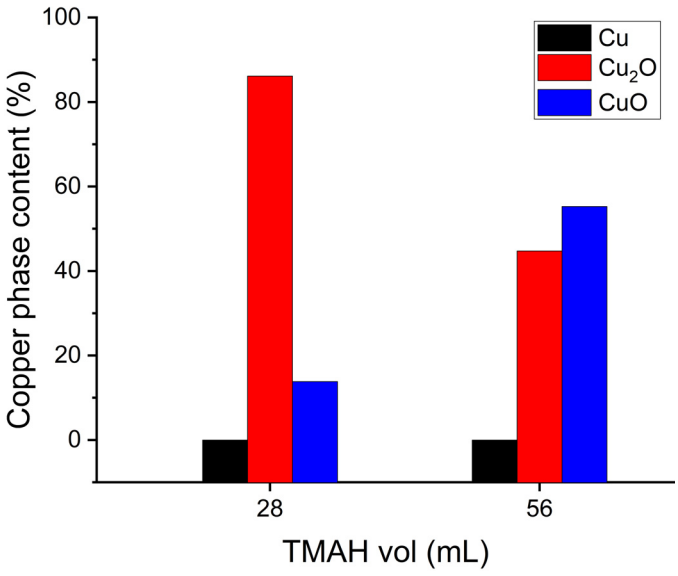

Fig. 5b. Abundance of copper species as a function of the TMAH amount

with the increase in temperature, while the amount of Cu_2O slightly increases. At 500°C elementary Cu appears, indicating that at higher temperatures lower Cu oxidation states are favoured. By analysing the evolution of crystal size for both copper oxides (Fig. 6b), the crystal growth is higher for CuO than for Cu_2O, which could indicate that the formation of Cu (I) or Cu (II) oxides is crystal size dependent. Thus, CuO is stable for crystal sizes below ~50 nm, Cu_2O between ~50 and 55 nm, and Cu above 55 nm. The calculated value from the XRD pattern of the sample calcined at 500°C was 103 nm.

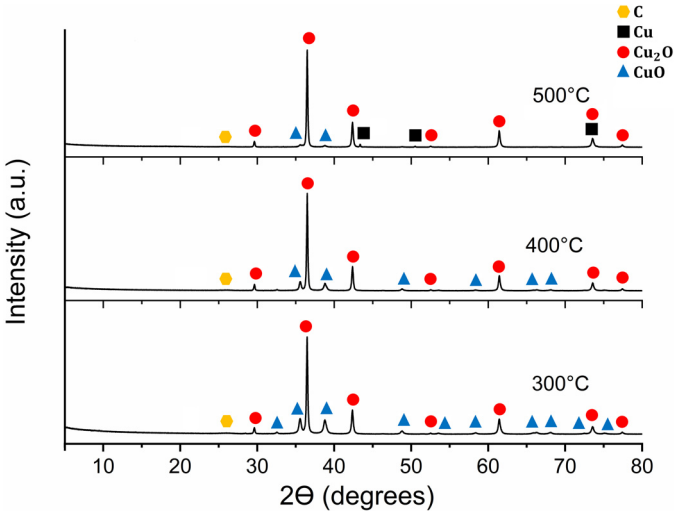

Fig. 6a. XRD patterns of the Cu-based/MWCNT composites

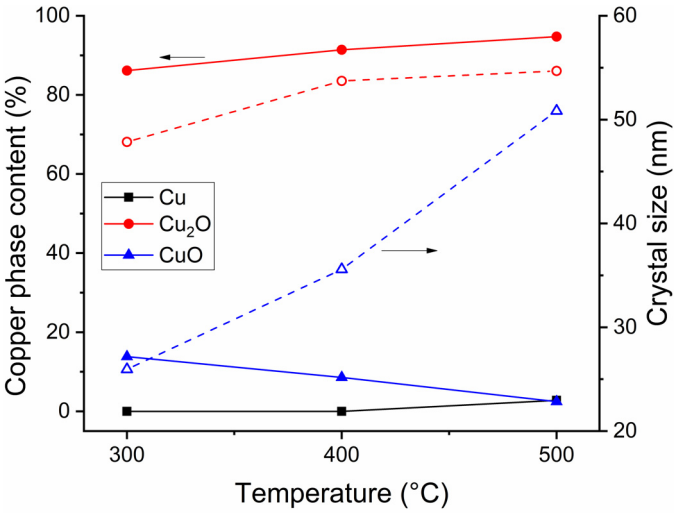

Fig. 6b. Abundance and crystal size of copper species as a function of calcination temperature

Based on those observations, the sample calcined at 300 °C was chosen for further analyses. In Figure 7 TEM images are shown, on which particles of a wide size range, i.e. from 5 to 100 nm, are clearly visible. Moreover, the nanoparticles interact well with the MWCNTs, which is desired for their retention in the filter.

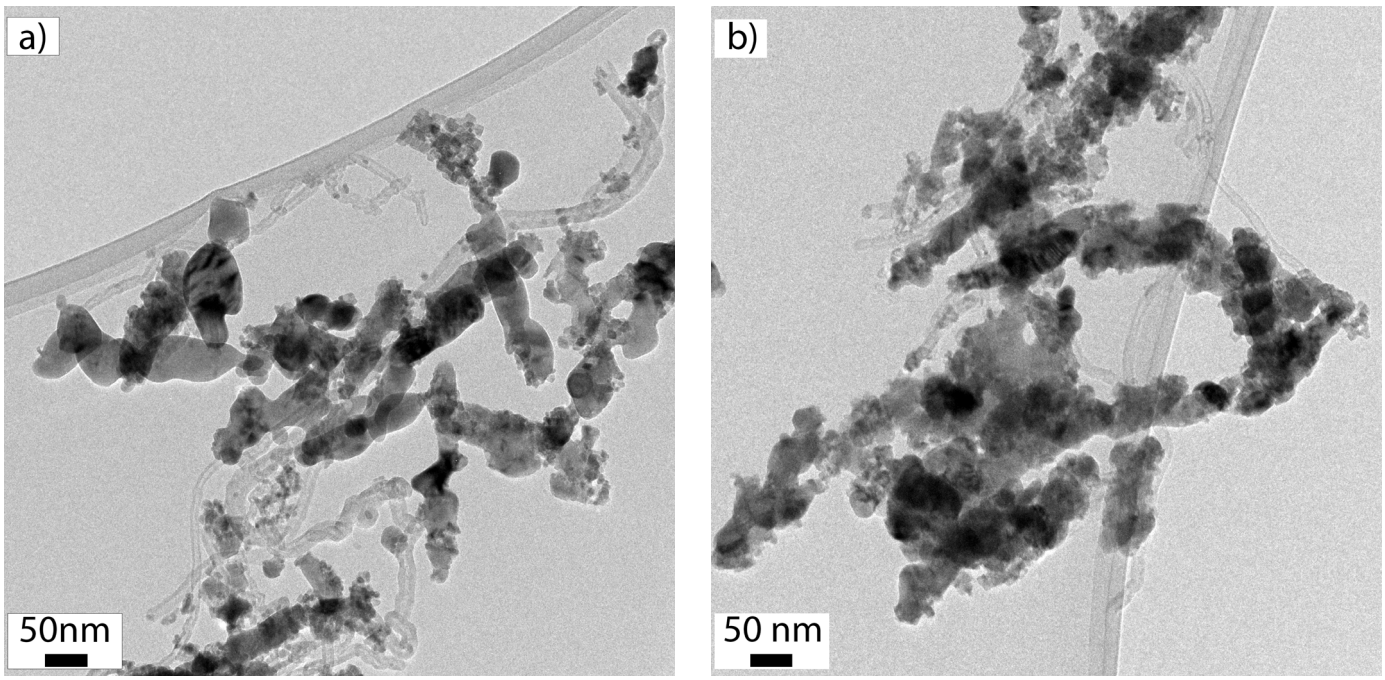

Fig. 7a and b. TEM images of the Cu-based composite obtained by stoichiometric precipitation reaction and after calcination at 300°C for 2 h under N2 atmosphere

3.3. Copper leakage

The study of copper release in the composite obtained after calcination at 300°C reveals that the amount of copper released after rinsing with 4 L of water at pH 5 was higher than for water at pH 7. The copper loss was measured to be 17.5 µg/L (0.17 mol%) and 7.3 µg/L (0.07 mol%) for the experiments run at pH 5 and 7, respectively. This phenomenon is caused by the higher solubility level of copper oxide at acidic pH values [30,31]. According to the World Health Organisation (WHO) [32], the maximum copper contents allowed in drinking water is 2 mg/L, therefore the produced filters could be potentially used for water filtration applications.

4. Conclusions

In this work, Cu-based MWCNT composites were synthesized via a simple chemical precipitation method. The use of stoichiometric amounts of TMAH leads to obtaining Cu_2O as the major phase (after calcination at 300°C under N_2 atmosphere), while an excess quantities of TMAH increase the CuO amount. It was observed that a lower Cu oxidation state is favoured with the increase in calcination temperature. TEM images show that the size of the copper oxide nanoparticles are between 5 and 100 nm and interact well with the MWCNTs. Finally, it was determined that copper leakage is higher at pH 5 (17.5 µg/L) than at pH 7 (7.3 µg/L), nevertheless in both cases these values are under the limit established by the WHO.

Acknowledgement

Authors would like to thank Mrs. Caroline Hain and Mr. Brian Sinnet for their help and collaboration.

REFERENCES

[1] A. Martínez-Ruiz, G. Alonso-Nuñez, Mater. Res. Bull. **43**, 1492-1496 (2008).
[2] S.C. Smith, D.F. Rodrigues, Carbon N. Y. **91**, 122-143 (2015).
[3] J.P. Kim, J.H. Kim, J. Kim, S.N. Lee, H.O. Park, J. Environ. Sci. (China) **42**, 275-283 (2016).
[4] Y.T. Ong, A.L. Ahmad, S.H.S. Zein, S.H. Tan, Brazilian J. Chem. Eng. **27**, 227-242 (2010).
[5] C. Liu, F. Wang, Q. Liang, J. Liu, Z. Chen, S.D. Wang, Ceram. Int. **42**, 17916-17919 (2016).
[6] Z. Németh, G.P. Szekeres, M. Schabikowski, K. Schrantz, J. Traber, W. Pronk, K. Hernádi, T. Graule, R. Soc. Open Sci. **6**, 181294 (2019).
[7] H. Chu, L. Wei, R. Cui, J. Wang, Y. Li, Coord. Chem. Rev. **254**, 1117-1134 (2010).
[8] S. Kang, M. Herzberg, D.F. Rodrigues, M. Elimelech, Langmuir **24**, 6409-6413 (2008).
[9] S. Kang, M.S. Mauter, M. Elimelech, S. Kang, M.S. Mauter, Langmuir **42**, 7528-7534, (2008).
[10] S. Kang, M. Pinault, L.D. Pfefferle, M. Elimelech, Langmuir **23**, 8670-8673, (2007).
[11] F. Yang, Q. Jiang, W. Xie, Y. Zhang, Chemosphere **185**, 162-170 (2017).

[12] A.S. Brady-Estévez, M.H. Schnoor, C.D. Vecitis, N.B. Saleh, M. Elimelech, Langmuir **26**, 14975-14982 (2010).
[13] A.S. Brady-Estévez, S. Kang, M. Elimelech, Small. **4**, 481-484 (2008).
[14] G.P. Szekeres, Z. Nemeth, K. Schrantz, K. Nemeth, M. Schabikowski, J. Traber, W. Pronk, K. Hernadi, T. Graule, ACS Omega **3**, 446-454 (2018).
[15] B. Michen, J. Fritsch, C. Aneziris, T. Graule, Environ. Sci. Technol. **47**, 1526-1533 (2013).
[16] V.K. Gupta, S. Agarwal, T.A. Saleh, Water Res. **45**, 2207-2212 (2011).
[17] V.K. Gupta, S. Agarwal, T.A. Saleh, J. Hazard. Mater. **185**, 17-23 (2011).
[18] O. Akhavan, R. Azimirad, S. Safa, M.M. Larijani, J. Mater. Chem. **20**, 7386-7392 (2010).
[19] J.D. Kim, H. Yun, G.C. Kim, C.W. Lee, H.C. Choi, Appl. Surf. Sci. **283**, 227-233 (2013).
[20] A. Ananth, S. Dharaneedharan, M.S. Heo, Y.S. Mok, Chem. Eng. J. **262**, 179-188 (2015).
[21] Y.J. Lee, S. Kim, S.H. Park, H. Park, Y.D. Huh, Mater. Lett. **65**, 818-820 (2011).
[22] H. Pang, F. Gao, Q. Lu, Chem. Commun. 1076-1078, (2009).
[23] X. Wang, B. Xia, X. Zhu, J. Chen, S. Qiu, J. Li, J. Solid State Chem. **181**, 822-827 (2008).
[24] X. Wang, F. Zhang, B. Xia, X. Zhu, J. Chen, S. Qiu, P. Zhang, J. Li, Solid State Sci. **11**, 655-659 (2009).
[25] P. Cui, A.J. Wang, J. Saudi Chem. Soc. **20**, 343-348 (2016).
[26] Y.F. Lim, J.J. Choi, T. Hanrath, J. Nanomater. (2012).
[27] J.H. Lehman, M. Terrones, E. Mansfield, K.E. Hurst, V. Meunier, Carbon N. Y. **49**, 2581-2602 (2011).
[28] E.F. Antunes, A.O. Lobo, E.J. Corat, V.J. Trava-Airoldi, A.A. Martin, C. Veríssimo, Carbon N. Y. **44**, 2202-2211 (2006).
[29] A. Jorio, R. Saito, G. Dresselhaus, M.S. Dresselhaus, Raman Spectroscopy in Graphene Related Systems, 2011.
[30] M. Pourbaix, Atlas of Electrochemical Equilibria in Aqueous Solutions, National Association of Corrosion Engineers, 1974.
[31] D.A. Palmer, P. Bénézeth, Solubility of Copper Oxides in Water and Steam, 2008.
[32] WHO, (2004). https://www.who.int/water_sanitation_health/water-quality/guidelines/chemicals/copper.pdf?ua=1 (accessed February 18, 2019).